

# Modeling and Control of a Hybrid Locomotion System

V. Krovi

Assistant Professor  
Department of Mechanical Engineering  
McGill University  
Montreal, Canada H3A-2K6  
venkat@cim.mcgill.ca

V. Kumar

Professor  
Department of Mechanical Engineering  
and Applied Mechanics  
University of Pennsylvania  
Philadelphia, PA 19104  
kumar@cis.upenn.edu

*This paper describes a hybrid mobility system that combines the advantages of both legged and wheeled locomotion. The legs of the hybrid mobility system permit it to surmount obstacles and navigate difficult terrain, while the wheels allow efficient locomotion on prepared surfaces and provide a reliable passive mechanism for supporting the weight of the vehicle. We address the modeling, analysis and control of such hybrid mobility systems using the specific example of a wheelchair with two powered rear wheels, two passive front casters, and two articulated, two-degree-of-freedom legs. We exploit the redundancy in actuation to actively control and optimize the contact forces at the feet and the wheels. Our scheme for active traction optimization redistributes the contact forces so as to minimize the largest normalized ratio of tangential to normal forces among all the contacts. Simulation and experimental results for the prototype are presented to demonstrate and evaluate the approach.*

## 1 Introduction

**1.1 Motivation.** Most land based mechanized locomotion systems are based on the principle of the wheel for two principal reasons. First, the wheels support the load passively requiring actuation only to propel the vehicle. Second, rolling contacts between the wheel and ground allow for efficient locomotion on flat prepared surfaces. However, the performance of wheeled systems is adversely affected by uneven terrain. In contrast, legged locomotion systems have the ability to pick footholds and to actively control the distribution of forces, and are therefore potentially more versatile (Hirose, 1984; Kumar and Waldron, 1989; Okhotsimski et al., 1977; Song and Waldron, 1989). In addition, actively controlled legs give the vehicle an active suspension.

However, legged vehicles are inefficient because the leg actuators must perform isometric work to support the weight of the vehicle, in addition to providing the tractive forces. A nonback-driveable transmission reduces the work requirements, but this makes it difficult to actively control the foot forces and to provide an active suspension. Further, while the reliability and stability of legged vehicles can be enhanced by increasing the number of legs, this is at the expense of increased complexity in design and control. These factors combine to make it very difficult to design a compact and reliable legged vehicle with a high payload to weight ratio.

Motivated by the above observations, we consider a hybrid vehicle that combines the use both legs and wheels (Kumar et al., 1996). The legs of this hybrid vehicle are used primarily on uneven terrain. Figure 1(A-D) shows the hybrid vehicle climbing a curb using a four-stage maneuver. When both the legs and wheels are powered, the system is redundantly actuated and the legs and wheels must "cooperate" to perform all maneuvers. A forward (or backward) motion may be accomplished by using the legs alone, or the powered rear wheels alone, or by using both concurrently. While the powered rear wheels are adequate for travel on prepared surfaces, the combined use of both legs and wheels, Fig. 1(E-F), can enhance traction, stability and safety on unprepared uneven surfaces. In addition, the legs can also be used to manipulate objects in the environment either individually, as shown in Fig. 1(G), or cooperatively as shown in Fig. 1(H). The key feature of the hybrid vehicle is that it operates in a statically stable configuration, while being

passively supported by the wheels. Since the legs are never required to support the entire weight of the vehicle, it is safer than a legged vehicle. Thus, the hybrid system can perform many tasks that can be accomplished by the traditional legged systems, and yet is simpler, safer and less expensive.

There are many applications for such a hybrid locomotion system. The design of a wheelchair with legs for people with disabilities is proposed in Wellman et al. (1995) and also described in this paper. A similar vehicle, but with wheels attached to the articulated legs, was proposed for forestry work by Hiller and Kecskemethy (1987). The ability to surmount obstacles, and to adapt to different terrain makes it attractive for applications in hazardous remote environments and unmanned planetary exploration (Kumar and Waldron, 1989).

Hybrid locomotion systems share two important characteristics with multilegged walkers with foot-ground contacts (and multifingered grippers with fingertip-object contacts). First, such systems rely on frictional contacts for stable support and successful locomotion (or manipulation). Second, the concurrent use of the actively controlled wheels and legs introduces redundancy in actuation, a situation in which the number of actuators exceeds the number of degrees of freedom of the system. This redundancy in actuation can be used to optimize and directly control the force distribution at the frictional point contacts. In multilegged walkers (and multifingered grippers) it is typically possible to control all components of forces at each contact. Both the force distribution problem and its solution are well understood (Ji and Roth, 1988; Kerr and Roth, 1986; Kumar and Waldron, 1988; Nguyen, 1987; Salisbury and Roth, 1983).

However, in a hybrid mobility system, it is possible to control only the tangential contact force at each powered wheel, and it is not possible to control any contact force at a passive wheel. This is also true for actively-controlled, articulated, wheeled vehicles (Hirose and Morishima 1990; Kumar and Waldron 1989; Sreenivasan and Waldron 1996). In this paper, we present the modeling and control of hybrid mobility systems, with some emphasis on our experimental wheelchair that is equipped with both legs and wheels.

Conventional motorized wheelchairs require prepared surfaces to locomote and cannot easily tackle the muddy patches, potholes or poor traction conditions encountered on sandy beaches, icy pavements and wooded parks. Special-purpose aids, like stair-climbers and customized outdoor buggies, solve specific problems but tend to be customized to a particular environment (Thring, 1983). Legs or other actively-controlled articulations have not been considered in wheelchair designs

Contributed by the Design Automation Committee for publication in the JOURNAL OF MECHANICAL DESIGN. Manuscript received Apr. 1997; revised Mar. 1999. Associate Technical Editor: B. Ravani

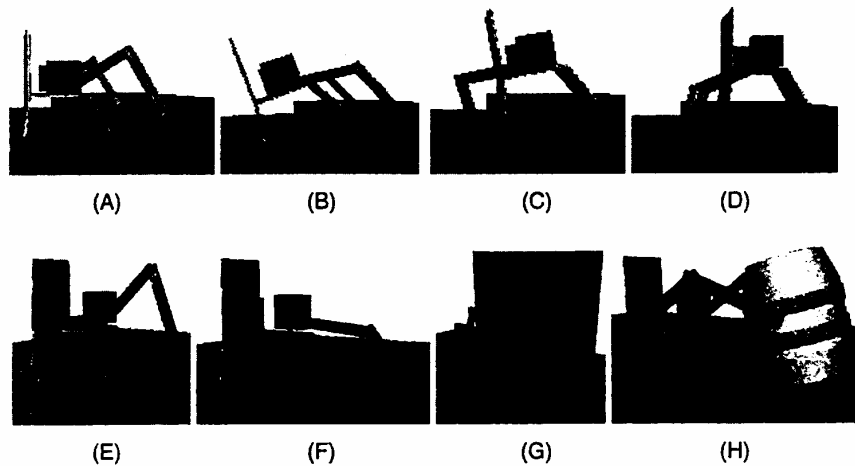


Fig. 1 (A–D) A curb climbing maneuver; (E, F) moving forward; (G) pushing open doors; and (H) manipulating objects (video footage available [www.cis.upenn.edu/~venkat/wheel.html](http://www.cis.upenn.edu/~venkat/wheel.html))

(with the sole exception of a four-legged prototype chair with non-backdriveable pantograph legs (Zhang and Song, 1989)) due to concerns of reliability and safety.

In Section 2, we describe the experimental prototype system. We discuss the kinematics and dynamics of the system in Section 3 and develop an active traction optimization scheme to optimize the locomotion characteristics of the system. In Section 4, we analyze the performance of this scheme with the help of both simulation and experimental studies. Section 5 concludes the paper.

## 2 Experimental Prototype of a Wheelchair with Legs

We begin with a brief description of our prototype hybrid wheelchair with legs shown in Fig. 2 and whose key dimensions are shown in Table 1.

Our prototype chair has a pair of two-degree-of-freedom planar legs with the provision of adding a third degree of freedom for out of plane motions. The two rear wheels are powered while the two front wheels are casters. The vehicle is constrained to operate in its sagittal plane (perpendicular to the rear axle) when its legs come in contact with the ground. However, the wheels permit the vehicle to move anywhere in the plane of the ground at all other times.

Each joint in the leg and each rear wheel is driven by a DC gear motor powered by 20 kHz PWM amplifiers that operate off a 24 volt DC power source, potentially two standard 12 volt lead-acid batteries. A parallel drive configuration, using a chain and sprocket transmission, allows the drive motors of each leg to be placed on the chassis reducing the overall power and torque requirements (compared to a conventional serial chain

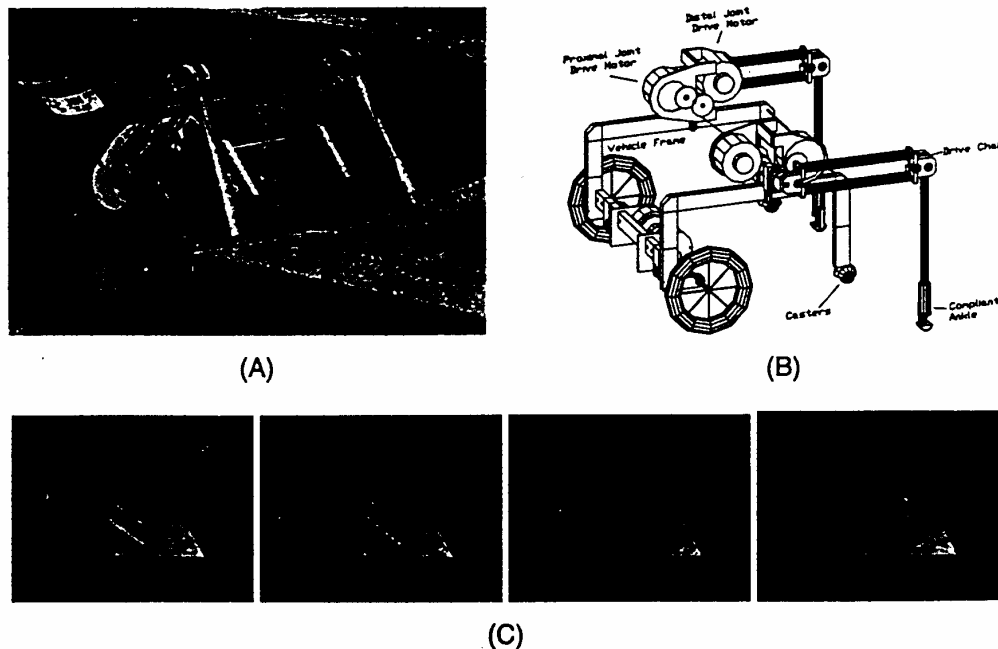


Fig. 2 (A) The experimental prototype; (B) CAD drawings of the wheelchair chassis; and (C) the four-stage curb climbing sequence

**Table 1 Optimal design parameters**

Design parameters	Values	Design parameters	Values
Weight (without batteries/payload)	28.2 kg. (62.0 lb.)	Length of Thigh/Upperarm	0.404 m. (15.9 in.)
Overall Width	0.775 m. (30.5 in.)	Weight of Thigh/Upperarm	1.02 kg. (2.25 lb.)
Wheelbase	0.533 m. (21.0 in.)	Length of Shank/Lowerarm	0.480 m. (18.9 in.)
Radius of Wheel	0.114 m. (4.5 in.)	Weight of Shank/Lowerarm	0.841 kg. (1.85 lb.)
Height of C.G.	0.191 m. (7.5 in.)	Maximum torque (Thigh/Upperarm)	67.80 Nm. (600 in-lb.)
Distance of C.G. from Rear Wheel	0.335 m. (13.2 in.)	Maximum Torque (Shank/Lowerarm)	67.80 Nm. (600 in-lb.)
Height of Shoulder Joint	0.305 m. (12.0 in.)	Maximum Wheel Torque	3.95 Nm. (35 in-lb.)
Distance of Shoulder Joint from Rear Wheel	0.267 m. (10.5 in.)		

configuration). The tension in the chain is sensed by strain gages, mounted on a special tensioning link of the chain, and used to compute one component of the foot force. The distal link is equipped with a compliant ankle, mounted on a linear bearing instrumented with a linear potentiometer, permitting the measurement of the axial foot force. All joint positions are measured directly at a resolution of 2500 counts per degree while velocity is computed digitally by taking successive derivatives of the position signal. The control computer is an IBM compatible 486 PC with an i860 coprocessor running concurrently. Further details of the mechanical design, the control system and the user interface can be found in Wellman et al. (1995) and Krovi (1995).

**3 Modeling and Control**

**3.1 Kinematics.** We will model and analyze the configuration of the hybrid wheelchair system described in Section 2. The actively controlled legs and wheels are capable of exerting forces only in the plane of the vehicle. Therefore, we consider

$$\mathbf{A}(\mathbf{q}) = \begin{bmatrix} 1 & \frac{S_\alpha}{C_\alpha} & -R/C_\alpha & 0 & 0 & 0 \\ \frac{-S_\alpha}{C_\alpha} & 1 & 0 & 0 & 0 & 0 \\ 1 & 0 & 0 & \begin{pmatrix} -N_c S_{\alpha\zeta 2} - L_3 S_{\alpha\zeta 23} \\ -L_4 S_{\alpha\zeta 234} \end{pmatrix} & \begin{pmatrix} -L_3 S_{\alpha\zeta 23} \\ -L_4 S_{\alpha\zeta 234} \end{pmatrix} & -L_4 S_{\alpha\zeta 234} \\ 0 & 1 & 0 & \begin{pmatrix} N_c C_{\alpha\zeta 2} + L_3 C_{\alpha\zeta 23} \\ + L_4 C_{\alpha\zeta 234} \end{pmatrix} & \begin{pmatrix} L_3 C_{\alpha\zeta 23} \\ + L_4 C_{\alpha\zeta 234} \end{pmatrix} & L_4 C_{\alpha\zeta 234} \end{bmatrix} \quad (6)$$

a planar, symmetric model of the system in which the two legs (and the two powered wheels) acts concurrently as shown in the maneuver in Fig. 2(C).

The wheelchair with a global inertial frame (OXY) and the key variables used in the modeling are depicted in Fig. 3. The overall system can be modeled as a four degree-of-freedom serial kinematic chain when the legs are not in contact with the

ground. The rear-wheel/ground contact forms the base joint, modeled as a rolling/gear pair with the wheel rotation denoted by  $\theta_1$ . The wheel axle, the hip joint, and the knee joints are modeled as revolute joints, with displacements denoted by  $\theta_2$ ,  $\theta_3$ , and  $\theta_4$ , respectively. The tip of the last link, the foot, is the end effector.

When the foot comes in contact with the ground, a simple closed kinematic chain is formed and the system is overconstrained. The configuration of the system can be described by the vector of Lagrangian coordinates:

$$\mathbf{q} = [x_w, y_w, \theta_1, \theta_2, \theta_3, \theta_4]^T \quad (1)$$

where  $(x_w, y_w)$  are the Cartesian coordinates of the wheel axle. We use a redundant set of Lagrangian coordinates (as opposed to a minimal set of generalized coordinates) for two reasons. First, this set of coordinates simplifies the modeling of both constrained and unconstrained cases. Second, using the framework of Lagrangian dynamics in the constrained case, we can obtain expressions for the contact forces directly from the multipliers corresponding to the constraints. If there is no slip at the wheel contact, the Cartesian positions of the center of mass of the chair and the foot contact in the inertial frame in this frame are given by:

$$x_{cg} = R\theta_1 C_\alpha - RS_\alpha + M_c C_{\alpha\eta 2} \quad (2)$$

$$y_{cg} = R\theta_1 S_\alpha + RC_\alpha + M_c S_{\alpha\eta 2} \quad (3)$$

$$x_f = R\theta_1 C_\alpha - RS_\alpha + N_c C_{\alpha\zeta 2} + L_3 C_{\alpha\zeta 23} + L_4 C_{\alpha\zeta 234} \quad (4)$$

$$y_f = R\theta_1 S_\alpha + RC_\alpha + N_c S_{\alpha\zeta 2} + L_3 S_{\alpha\zeta 23} + L_4 S_{\alpha\zeta 234} \quad (5)$$

where,  $C_{xij}$  and  $S_{xij}$  denote  $\cos(x + \theta_i + \theta_j)$  and  $\sin(x + \theta_i + \theta_j)$ . The angle  $\theta_1 - \theta_2$  is measured by an encoder at the wheel motor, while  $\theta_3$  and  $\theta_4$  are measured by encoders mounted at the leg motors. In the constrained case, if there is no slip at the foot, the foot coordinates  $(x_f, y_f)$  are constant. The determination of the unknown variables using inverse kinematics, given the closure equations above, is straightforward (Krovi, 1995).

**3.2 Dynamics.** Because the unconstrained case is modeled by standard kinematic and dynamic equations that are typical for serial chains, we consider only the constrained case below. We can collectively express the constraints in Eqs. (2-5) at the velocity level in matrix form:

$$\mathbf{A}(\mathbf{q})\dot{\mathbf{q}} = \mathbf{0}$$

where,

Because  $\mathbf{A}(\mathbf{q})$  is full rank, the overall system has two degrees of freedom. We can define a  $6 \times 2$  matrix,  $\mathbf{S}(\mathbf{q})$ , whose columns are any two vectors that span the null space of  $\mathbf{A}(\mathbf{q})$ . These columns constitute the "feasible" motion directions of the constrained system so that we can write:

$$\dot{\mathbf{q}} = \mathbf{S}(\mathbf{q})\mathbf{v}(t) \quad (7)$$

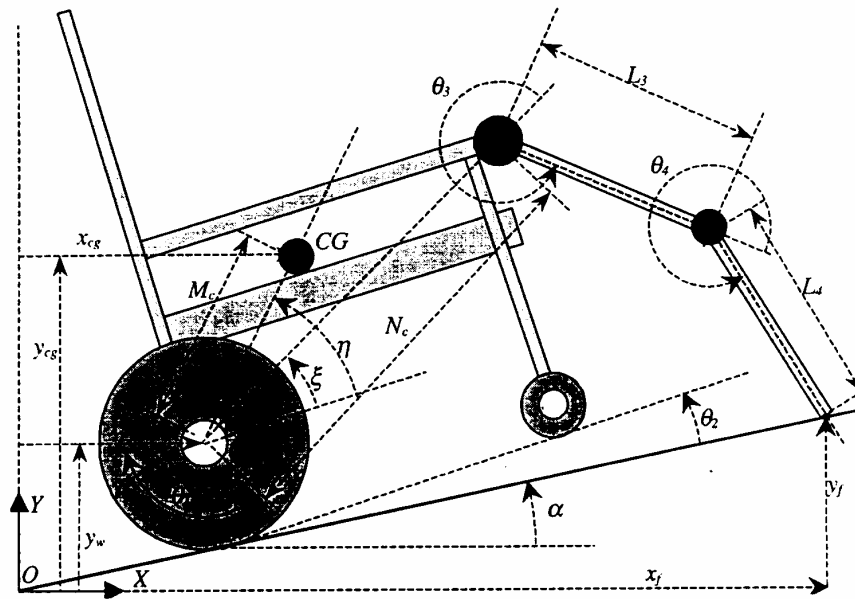


Fig. 3 Schematic of the wheelchair with modeling variables

where  $\mathbf{v} = [v_1, v_2]^T$  is a vector of generalized speeds for the system. We select  $\mathbf{v}$  to be the Cartesian velocities of the center of mass of the chair and accordingly define  $\mathbf{S}(\mathbf{q})$ . The dynamic equations of the constrained mechanical system can then be written as,

$$\mathbf{H}(\mathbf{q})\dot{\mathbf{q}} + \mathbf{h}(\mathbf{q}, \dot{\mathbf{q}}) = \mathbf{E}(\mathbf{q})\boldsymbol{\tau} - \mathbf{A}^T\boldsymbol{\sigma} \quad (8)$$

where  $\mathbf{H}$  is the  $6 \times 6$  inertia matrix,  $\mathbf{h}$  is a  $6 \times 1$  vector modeling the Coriolis, centripetal, gravity and frictional drag forces,  $\boldsymbol{\tau} = [\tau_1, \tau_2, \tau_3]^T$  is the  $3 \times 1$  vector of applied actuator forces,  $\boldsymbol{\sigma} = [\sigma_1, \sigma_2, \sigma_3, \sigma_4]^T$  is the  $4 \times 1$  vector of Lagrange multipliers, and

$$\mathbf{E} = \begin{bmatrix} 0 & 0 & 1 & 1 & 0 & 0 \\ 0 & 0 & 0 & 0 & 1 & 0 \\ 0 & 0 & 0 & 0 & 1 & 1 \end{bmatrix}^T$$

is a  $6 \times 3$  matrix that maps actuator forces to the generalized forces. Details of the empirical model for the frictional drag

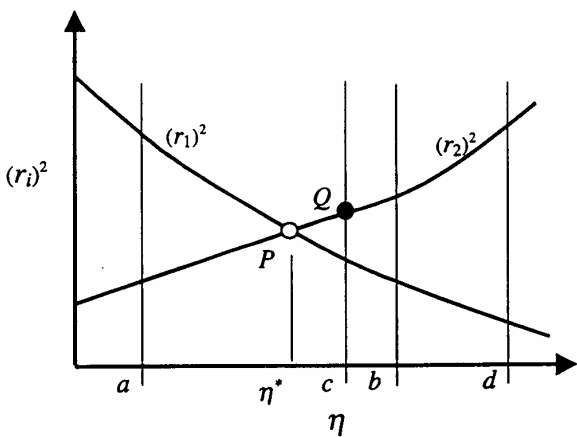


Fig. 4 Dependence of the traction ratios on the free variable

forces are discussed in Krovi and Kumar (1995) and Krovi (1995).

Differentiating Eq. (7), substituting for  $\dot{\mathbf{q}}$  into Eq. (8), pre-multiplying by  $\mathbf{S}^T$  and rearranging terms we get:

$$\dot{\mathbf{v}} = -(\mathbf{S}^T\mathbf{H}\mathbf{S})^{-1}[(\mathbf{S}^T\mathbf{H}\dot{\mathbf{S}}\mathbf{v} + \mathbf{S}^T\mathbf{h})] + (\mathbf{S}^T\mathbf{H}\mathbf{S})^{-1}\mathbf{S}^T\mathbf{E}\boldsymbol{\tau} \quad (9)$$

Equation (9) gives us expressions for the two accelerations (derivatives of generalized speeds) in terms of the applied actuator forces. Explicit analytical equations for the multipliers in terms of the applied actuator forces can be found by differentiating Eq. (7) and eliminating  $\dot{\mathbf{q}}$  in favor of  $\boldsymbol{\sigma}$  from Eq. (8):

$$\boldsymbol{\sigma} = (\mathbf{A}\mathbf{H}^{-1}\mathbf{A}^T)^{-1}[\dot{\mathbf{A}}\mathbf{S}\mathbf{v} - \mathbf{A}\mathbf{H}^{-1}\mathbf{h}] + (\mathbf{A}\mathbf{H}^{-1}\mathbf{A}^T)^{-1}\mathbf{A}\mathbf{H}^{-1}\mathbf{E}\boldsymbol{\tau} \quad (10)$$

The individual components of  $\boldsymbol{\sigma}$  can be identified with the constraint forces associated with each equation of constraint. Specifically,  $\sigma_1$  and  $\sigma_2$  are the tangential and normal wheel forces while  $\sigma_3$  and  $\sigma_4$  correspond to the tangential and normal foot forces. It is clear from Eq. (9) that the two acceleration variables are an affine function of the three motor torques. For a desired trajectory, there are infinite torque vectors, lying in the null space of the coefficient matrix,  $(\mathbf{S}^T\mathbf{H}\mathbf{S})^{-1}\mathbf{S}^T\mathbf{E}$ , that will satisfy Eq. (9). The active traction optimization scheme developed in the next section addresses the optimal selection of the torques for a specified trajectory.

**3.3 Active Traction Optimization.** In order to prevent slip and to maintain contact we require:

$$F_{n,i} \geq 0 \quad i = 1, 2 \quad (11)$$

$$|F_{t,i}| \leq \mu_i |F_{n,i}| \quad i = 1, 2 \quad (12)$$

where  $i$  denotes the  $i^{\text{th}}$  contact and  $F_n$  and  $F_t$  denote the normal and tangential force components. The traction ratio,  $r_i$ , is defined as the ratio of the tangential force to the normal force at contact  $i$ , normalized by the friction coefficient  $\mu_i$  (Johnson et al., 1991):

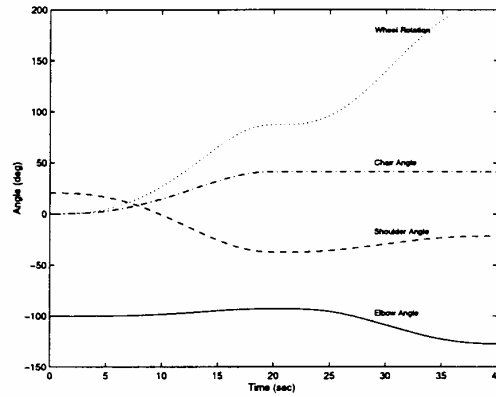
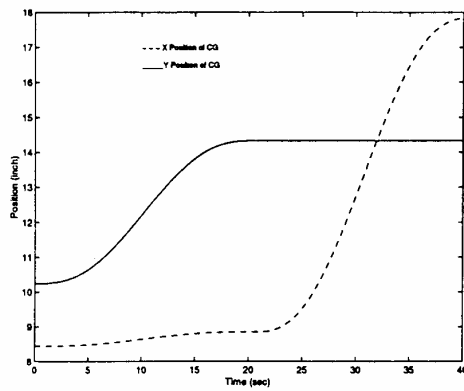


Fig. 5 Desired motion: Cartesian trajectory of the center of gravity (left) and joint trajectories (right)

$$r_i = \frac{F_{i,d}}{\mu_i F_{n,i}} \quad (13)$$

Slip occurs when  $|r_i| = 1$ . As the value of  $|r_i|$  becomes smaller, the tendency to slip reduces.

We propose an active traction optimization scheme to exploit the redundancy in actuation to minimize the largest traction ratio to find the optimal torques:

$$\min [\max (r_1^2, r_2^2)], \quad |\tau| \leq \tau_{\max} \quad (14)$$

subject to the constraints in Eqs. (9, 10, 11, 13). The  $\dot{v}$  in Eq. (9) is obtained from the specifications of the desired trajectory and  $\tau_{\max}$  is the vector of actuator torque limits. From Eq. (9), we can write the torques in terms of the specified accelerations in the form:

$$\tau = [(S^T H S)^{-1} S^T E]^+ (S^T H S)^{-1} [(S^T H \dot{S} v + S^T h)] + [(S^T H S)^{-1} S^T E]^+ \dot{v} + \eta \tau_h \quad (15)$$

where  $[\cdot]^+$  is the generalized inverse of  $[\cdot]$ ,  $\tau_h$  is a vector that belongs to the null space of the coefficient matrix,  $(S^T H S)^{-1} S^T E$ , and  $\eta$  is a free variable in the optimization.

The optimization over  $\eta$  is illustrated in Fig. 4. Let  $P$  be the point at which the  $(r_1)^2$  versus  $\eta$  curve intersects the  $(r_2)^2$  versus  $\eta$  curve. When there are no limits on  $\eta$ , the value of  $\eta = \eta^*$  is optimal because  $(r_1)^2 = (r_2)^2$ . Any deviation of  $\eta$  from this optimal value will result in one of the traction ratios becoming larger. This unconstrained problem is obtained by substituting Eq. (15) and the condition  $(r_1)^2 = (r_2)^2$  into Eq. (10), and solving the resulting quartic in  $\eta$  (Krovi, 1995). The quartic yields four roots, and the best feasible solution is quickly found by inspection.

When the actuator torque limits are mapped into limits on the free variable  $\eta$ , we get the two cases (Johnson et al., 1991). In Case (A) the allowable interval, typified by  $[a, b]$ , includes the point  $P$ , and in Case (B) the allowable interval, typified by  $[c, d]$ , does not include the point  $P$  in Figure 4. In Case (A), it is easy to see that  $P$  remains the optimal point, and is solved as discussed above. In Case (B), one of the ends of the interval ( $Q$  in the figure) becomes the optimal point. By substituting this value (either  $c$  or  $d$ ) in Eq. (15), we get the optimal torques.

In the physical implementation in our prototype, the optimization problem is solved in two stages. We first solve the quartic from the unconstrained problem and check to see if the obtained solutions for the actuator torques satisfy the actuator limits. If the limits are violated, we solve Eq. (9) with the corresponding torque set to its limit. Since there are only  $2^3 = 8$  cases for three

actuators, all the solutions are easily computed and compared to find the optimal torques in real time.

## 4 Performance Evaluation

**4.1 Simulation Results.** We first discuss the results of simulation studies, carried out using MATLAB, with varying step sizes and stride lengths. A sample desired motion trajectory, for half of a step-climbing maneuver, is shown in Fig. 5. The front wheels of the prototype wheelchair are lifted onto a 0.3556 m. (14 in.) step in two, 20 second motion phases. In the first phase, the front wheels are lifted 0.3556 m. (14 in.) off the ground and moved forward by 0.0254 m. (1 inch). In the second phase, the front wheels are maintained at the same height and moved forward by 0.2286 m. (9 in.). A minimum jerk trajectory is created in each phase to accomplish the motion. All the results in this section are presented for this desired trajectory. Note also that the actual motion is identical to the desired motion in simulations but not in the experimental case discussed later.

We discuss the simulation results for three cases: (A) the system without actuator redundancy, where the arms alone accomplish the curb-climbing maneuver without actuating wheel motors; (B) the system with actuator redundancy where the wheel motors are used along with the leg motors in the active traction optimization paradigm; and (C) The system with actuator redundancy and active traction optimization but with actuator limits imposed on the wheel motor. In the left column of Fig. 6, we depict the force histories—normal forces (solid lines) and tangential forces (dashed)—at each contact. In the right column, we depict the corresponding ratios for each of the three cases.

In Case (A), all the tractive forces are provided by the legs while the wheel motors are inactive. We observe that a very large traction ratio at the foot, while the tangential force and the traction ratio at the wheel are zero. In Case (B), the tangential (tractive) forces are redistributed between the wheels and legs. The traction ratio at the foot reduces from around 0.9 in Case (A) to about 0.3 in Case (B), while the traction ratio at the wheel increases from 0 to around 0.3. The important thing to note is the traction ratios are now equal (and therefore optimal) at all times during the maneuver. In Case (C), the required wheel torque for complete traction optimization exceeds the actuator's limits. Hence, we set the wheel torque to its limiting value and recompute the leg actuator torques from Eq. (9). As seen in Fig. 6(C), the wheels still provide some tractive force which is inadequate to achieve complete traction optimization. Nevertheless, the perfor-

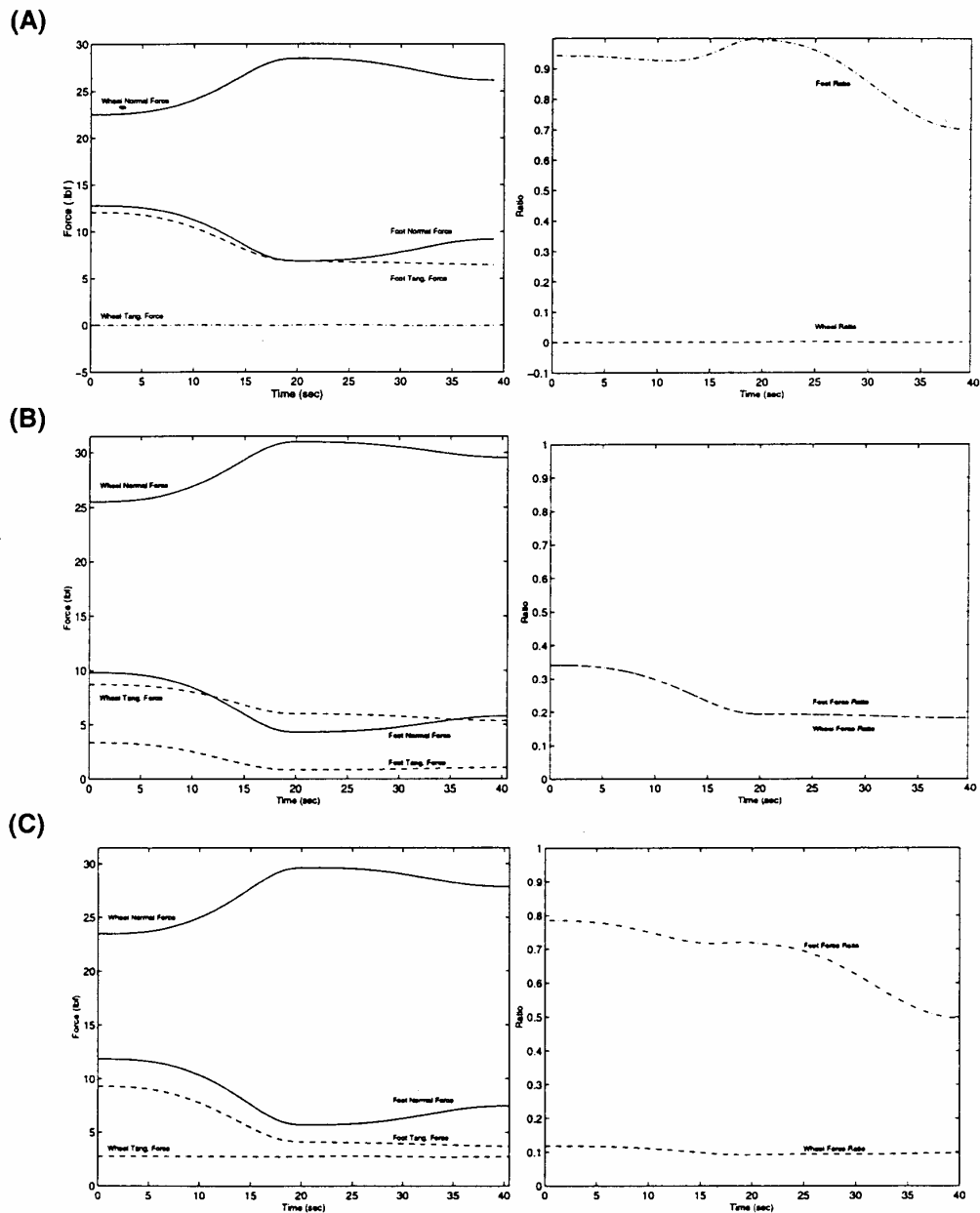


Fig. 6 Simulation results with force histories (left) and traction ratios (right) for each of the three cases: (A) System without actuator redundancy; (B) System with actuator redundancy and active traction optimization; (C) System with actuator redundancy, traction optimization and torque limits on the wheel motor

mance is superior to that shown in Fig. 6(A). The traction ratios are below 0.8 through out the maneuver. The detailed parametric study performed to study the effects of varying the actuator limits is presented in Krovi (1995).

**4.2 Experimental Results.** Experimental studies were conducted with the prototype vehicle under the same conditions as in the last simulation study. The prototype was controlled using the active traction optimization scheme in the presence of wheel actuator limits. The resulting experimental forces were recorded by an independent data collection system. In Fig. 7, these experimental forces and the traction ratios are shown (in

solid lines), superposed over the simulation results of Fig. 6(C) (in dotted lines). There is general agreement between the predicted (simulated) and the observed (experimental) data. The foot does not exhibit any noticeable slip even though the traction ratios are relatively high because the experiments were performed a high friction rubber foot on a carpeted floor. The observed joint trajectories from the experimental prototype are shown in Fig. 7(C) (superposed over the desired joint trajectories from Fig. 5(B)). We note that the wheel rotation lags the desired trajectory slightly because the wheel motors saturate.

There are several reasons for the noise in the experimental results and the discrepancies with the predictions. First, the

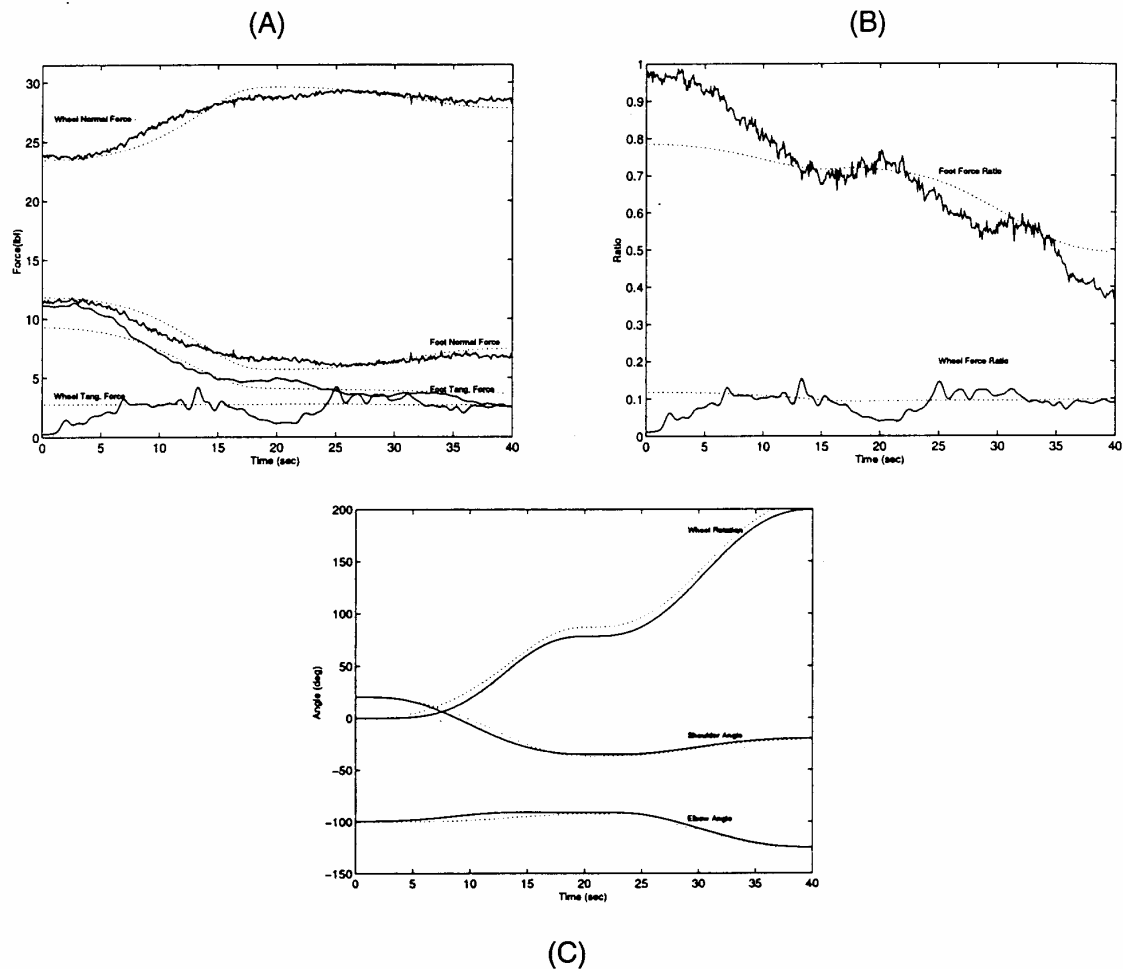


Fig. 7 Experimental results (solid lines) superposed on simulation results (dotted lines) for the system with actuator redundancy, traction optimization and wheel torque limits: (A) Force histories; (B) Traction ratios; (C) Joint trajectories

wheel forces are inferred by subtracting the foot force from the weight of the vehicle, based on a static model of the system. The dynamics of the system induce errors in the estimates of the wheel contact forces despite the low operational speeds. Second, because the wheel contact forces are not explicitly measured, we cannot close a feedback loop around the forces which adversely affects the performance of the system. Other sources of error, including friction and the non-collocation of sensors and actuators are further discussed in Krovi (1995).

## 5 Conclusions

In this paper, we propose a novel approach to locomotion in unstructured environments called hybrid locomotion which combines the advantages of wheeled and legged locomotion. Our prototype hybrid wheelchair with legs can climb 0.3556 m. (14 in.) high obstacles (like curbs), ascend (or descend) 30 degree inclines, navigate omnidirectionally using only its wheels on planar surfaces and using both wheels and legs on "difficult" terrain.

The second main contribution of the paper is an optimal traction scheme for mechanical systems with actuator redundancy and actuator limits. A new method, called active traction optimization, was developed and implemented for resolving the

redundancy in actuation. This method optimizes the force distribution and reduces the tendency to slip. Experimental and simulation studies for curb climbing with our prototype system demonstrate and evaluate the approach.

## Acknowledgments

We acknowledge the Whitaker Foundation and the National Science Foundation (grants CMS 91-57156, CISE/CDA 88-22719 and MIP 94-20397) for supporting the different aspects of this work.

## 6 References

- Hiller, M., and Keckemethy, A., 1987, "A Computer-oriented Approach for the Automatic Generation and Solution of the Equations of Motion for Complex Mechanisms," *Proc. 7th World Congress on the Theory of Machines and Mechanisms*, Sevilla, Spain.
- Hirose, S., 1984, "A Study of Design and Control of a Quadruped Walking," *International Journal of Robotics Research*, Vol. 3, No. 2, pp. 113-133.
- Hirose, S., and Morishima, A., 1990, "Design and Control of a Mobile Robot with an Articulated Body," *International Journal of Robotics Research*, Vol. 9, No. 2, pp. 99-114.
- Ji, Z., and Roth, B., 1988, "Direct Computation of Grasping Force for Three-Finger Tip-Prehension Grasps," *ASME JOURNAL OF MECHANISMS, TRANSMISSIONS, AND AUTOMATION IN DESIGN*, Vol. 110, No. 4, pp. 405-413.

- 5 Johnson, L., Kumar, V., and Gardener, J. F., 1991, "Optimization of Contact Forces in Multi-fingered and Multi-legged Robots," *Proc. 2nd Ann. Applied Mechanisms and Robotics Conference*, Vol. 2.
- 6 Kerr, J., and Roth, B., 1986, "Analysis of Multifingered Hands," *International Journal of Robotics Research*, Vol. 4, No. 4, pp. 3-17.
- 7 Krovi, V., 1995, "Modeling and Control of a Hybrid Locomotion System," M.S. Thesis, Department of Mechanical Engineering, University of Pennsylvania, Philadelphia, Pennsylvania, URL: <http://www.cis.upenn.edu/~venkat/Publications.html>.
- 8 Kumar, V., and Waldron, K. J., 1988, "Force Distribution in Closed Kinematic Chains," *IEEE Transactions on Robotics and Automation*, Vol. 4, No. 6, pp. 657-664.
- 9 Kumar, V., and Waldron, K. J., 1989, "Actively Coordinated Vehicle Systems," *ASME JOURNAL OF MECHANISMS, TRANSMISSIONS, AND AUTOMATION IN DESIGN*, Vol. 111, No. 2, pp. 223-231.
- 10 Kumar, V., Wellman, P., and Krovi, V., 1996, "Adaptive Mobility System," U.S. Patent 5,513,716.
- 11 Nguyen, V. D., 1987, "Constructing Force-Closure Grasps," *Proc. 1987 IEEE Int. Conf. on Robotics and Automation*, Raleigh, CA, pp. 240-245.
- 12 Okhotsimski, D. E., Gurfinkel, V. S., Devyanin, E. A., and Platonov, A. K., 1977, "Integrated Walking Robot Development," *Machine Intelligence*, V9., Eds. J. E. Hayes, D. Michie and L. J. Mikulich.
- 13 Salisbury, J. K., and Roth, B., 1983, "Kinematic and Force Analysis of Articulated Mechanical Hands," *ASME JOURNAL OF MECHANISMS, TRANSMISSIONS AND AUTOMATION IN DESIGN*, Vol. 105, No. 1, pp. 35-41.
- 14 Song, S. M., and Waldron, K. J., 1989, *Machines that Walk*, MIT Press, Cambridge MA.
- 15 Sreenivasan, S. V., and Waldron, K. J., 1996, "Displacement Analysis of an Actively Articulated Wheeled Vehicle Configuration with Extensions to Motion Planning on Uneven Terrain," *ASME JOURNAL OF MECHANICAL DESIGN*, Vol. 118, No. 2, pp. 312-320.
- 16 Thring, M. W., 1983, *Robots and Telechairs: Manipulators with Memory, Remote Manipulators, Machine Limbs for the Handicapped*, Ellis Horwood; New York: Halsted Press.
- 17 Wellman, P., Krovi, V., Kumar, V., and Harwin, W., 1995, "Design of a Wheelchair with Legs for People with Motor Disabilities," *IEEE Transactions on Rehabilitation Engineering*, Vol. 3, No. 4, pp. 343-353.
- 18 Zhang, C-D., and Song, S. M., 1989, "Gaits and Geometry of a Walking Chair for the Disabled," *Journal of Terramechanics*, Vol. 26, No. 314, pp. 211-233.